Nanoscale

Accepted Manuscript

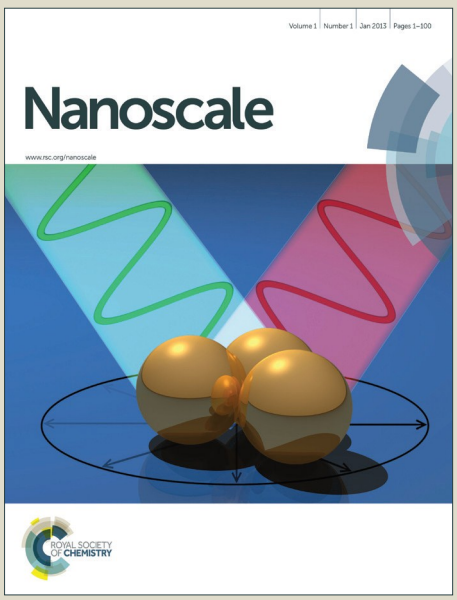

ROYAL SOCIETY OF CHEMISTRY

www.rsc.org/nanoscale

Table of contents text and graph.

Gold nanocorals (AuNC) are obtained by a "green" method consisting in laser irradiation followed by anisotropic self-assembly without templating agents. The AuNC dispersion has broadband plasmon absorption from visible to near infrared, unitary light-to-heat conversion efficiency, versatile surface chemistry and biocompatibility.

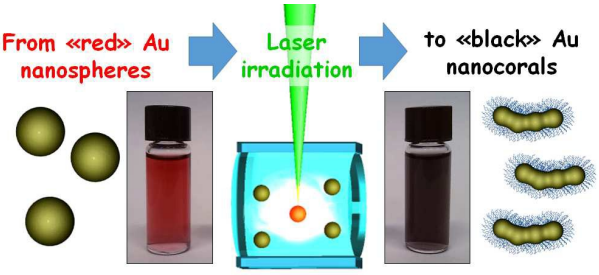

Introduction

Gold nanostructures play a prominent role in nanoscience and nanotechnology for their peculiar physical and chemical properties.[1] Among the favorable characteristics of gold nanoparticles, there are the intense extinction bands originated by the localized surface plasmon resonances (SPR), the generation of surface enhanced Raman scattering (SERS), the easy functionalization with a wide series of organic molecules, the high chemical and physical stability and the intrinsic biocompatibility of this metal.[1-4] Several types of gold nanostructures have been obtained to date, from the simplest case of nanospheres (NS) to more complex shapes such as nanoshells, nanorods, nanoprisms, nanopiramids and nanocages.[3, 4] Symmetry reduction in gold nanoparticles is an effective way to modify position, number and intensity of the SPR.[5-8] For instance, AuNS with size of 4 – 50 nm show only one plasmon band centered at about 520 nm, while a second, more intense and red shifted band appears when the symmetry is reduced from spherical to cylindrical, i.e. in Au nanorods.[6, 9] In particular, by increasing the aspect ratio of nanorods, the second SPR can be shifted from the visible to the near infrared (NIR) range.[10] In most Au nanostructures, however, the absorption bandwidth is limited to a small portion of the visible-NIR range due to the resonant nature of the plasmon excitation.[6, 8] Recently, asymmetric networks of gold nanoparticles have been proposed as an interesting system to obtain versatile and multimodal plasmonic responses.[11-13] For instance, networks of partially fused gold nanoparticles showed very low-energy surface plasmon modes capable of supporting long-range and spectrally tunable propagation in nanoscale waveguides.[11] These Au nanonetworks belong to the C_1 point group, that with lowest symmetry for an isolated object, hence the number of allowed SPR is larger compared to nanoparticles with higher symmetry. The interest in 1D Au nanoassemblies is due also to the their potential exploitability as intermediate steps for the fabrication of nanowires.[11, 14, 15]

Noble metal nanostructures with small size are important because they behave as pure plasmon absorbers, i.e. as nano-objects where the scattering cross section is negligible compared to the absorption cross section.[6, 9, 16] There is a long list of applications possible for Au nanostructures with efficient absorption in the visible and NIR, such as in light induced vapour generation,[17] plasmon enhanced catalysis,[18] photothermal polymerization,[19] antimicrobial systems,[20, 21] photoacoustic imaging,[22, 23] light triggered drug release[24, 25] and photothermal therapy.[10, 26, 27] For instance, the recent theoretical prediction of efficiencies up to 85% is fostering the development of plasmon thermophotovoltaic systems based on materials which are chemically stable at high temperatures and have broadband optical absorption.[28, 29] Generally, optical resonances in the NIR are useful for biological applications because skin, tissues, haemoglobin and blood have a transmission window with a peak at approximately 800 nm.[26] For instance, NIR absorbing nanoparticles are exploitable as

sensitizers for photothermal therapy, which is based on the occurrence of protein denaturation and cellular membrane disruption, with initiation of apoptotic mechanisms, when tissues temperature exceeds 42 – 44 °C.[26] Perfusion and oxygenation of tissues are also favoured by moderate heating, which is useful to improve the delivery of cytostatic drugs.[27] Besides, NIR absorbers are exploitable as contrast agents for photoacoustic imaging, which is rapidly emerging as a promising high-resolution technique for optical visualization of tissues.[22, 23] A key empowering feature in this field is the development of broadband red-NIR contrast agents for multispectral photoacoustic imaging.[23]

The ability to conjugate Au nanoparticles with functional organic molecules is very important for most of the above mentioned applications.[3, 12, 21, 30-32] For instance, surface functionalization is required for the colloidal stability in biological fluids or in liquid solution,[3, 33] the inclusion in polymeric matrixes,[19, 21] the addition of selectivity versus target biomolecules or other chemical species,[3, 30] and the formation of surface patterns with multiple applications.[34]

On the other hand, the surface of nanoparticles should be as clean as possible from undesired compounds in most biological and catalysis applications. In particular, one should avoid the presence of synthesis byproducts, stabilizing agents or templating molecules with toxic effects, or of any chemical compounds forming an undesired shell around nanoparticles.[33] For instance, the removal of cetyl trimethylammonium bromide (CTAB) from Au nanorods is required to reduce cytotoxicity prior to bioapplications.[33, 35, 36] Sometimes, templating agents interfere with the complete surface conjugation of gold nanoparticles, also because the replacement of CTAB by thiolated ligands may cause the destabilization of the colloidal system leading to aggregation.[3, 37-39]

Here we report the laser assisted synthesis of gold nanoparticles with small size, asymmetric elongated shape similar to nanocorals (AuNC) and endowed with broadband plasmon absorption from the visible to the NIR. Laser irradiation (LI) initiate the formation of AuNC by photofragmentation of AuNS dispersed in water/ethanol solution, previously obtained by laser ablation without any chemical or stabilizers. After laser fragmentation, Au nanocrystals spontaneously prosecute their growth by unidirectional assembly in solution, as a consequence of the balance between the electrostatic repulsive force and the attractive dipolar interactions in the colloidal system. The laser assisted approach introduces several benefits such as the synthesis under continuous flow, the environmentally friendly procedure without chemicals, stabilizers or templating molecules, the biocompatibility, the easy surface functionalization of products, and the limited size of nanostructures compatible with pure plasmon absorbers. AuNC, coated in one step with biopolymers, show excellent photothermal performances in the visible-NIR range both in liquid solution or after inclusion in polymeric matrixes. Besides, the safe-by-design of AuNC was assessed by *in-vitro* experiments which showed the absence of cytotoxic effects even at high

nanoparticles dose. Overall, the results suggest that AuNC are eligible candidates for multiple photothermal applications.

Results

In the typical synthetic procedure, spherical Au nanoparticles dispersed in water:ethanol 1:1 are fluxed in a glass channel, while the pulses of a ns laser (532 nm, 10 Hz, 1300 mJ/cm^2) are focused at normal incidence with flux direction (Figure 1a). Laser pulses are resonant with the SPR of Au nanospheres, which are photofragmented into AuNC with smaller size and asymmetric shape after absorption of laser light (Figure 1b). Noticeably, by ageing the irradiated solution for 7 days at 20 °C, the longitudinal size of AuNC increased, without appreciable changes in their transversal size. However, nanoparticles remain stable in the liquid dispersion also several weeks after LI. Dimensional analysis (Figure 1c) shows that pristine AuNS have size of 9 ± 5 nm, while AuNC at 0 and 7 days after LI have a lower transversal size of, respectively, 5 ± 1 nm and 5 ± 2 nm. Conversely, the longitudinal size of Au nanoparticles is 10 ± 4 nm and 15 ± 8 nm at, respectively, 0 and 7 days after LI. Importantly, the aspect ratio changes from 1.2 ± 0.3 in pristine AuNS to 2.2 ± 1.1 and 3.1 ± 1.8 in AuNC at, respectively, 0 and 7 days after LI.

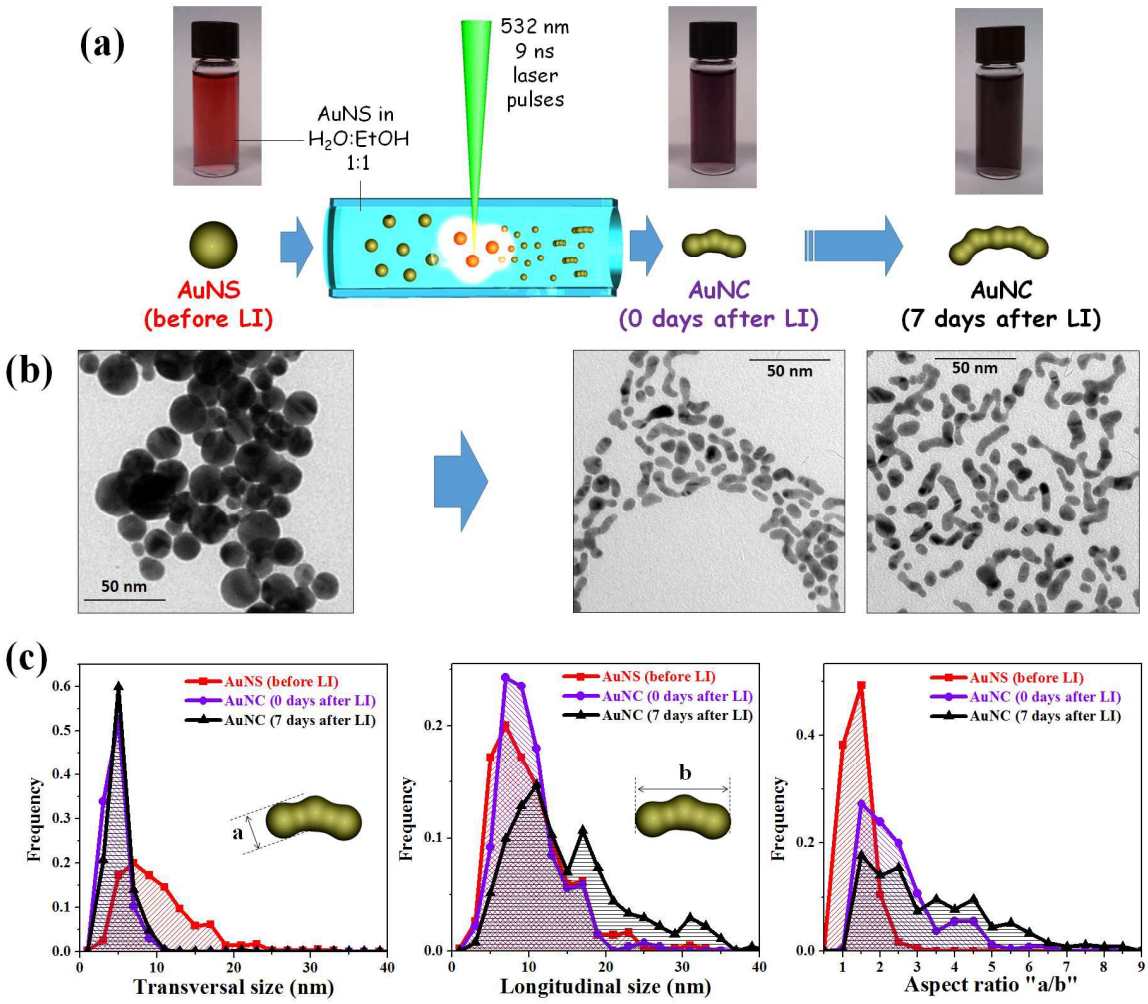

Figure 1. a) Sketch of the LI process exploited for the conversion of AuNS (red colloid in the vial on the left) into AuNC (violet colloid, in the middle). After ageing of the laser irradiated colloid for 7 days, the colloid became black (vial on the right). b) TEM images of AuNS (before LI, on the left) and of AuNC at day 0 and 7 after LI (middle and right figures, respectively). c) Histograms of Au nanoparticles transversal size ("a", left), longitudinal size ("b", middle), and aspect ratio ("b/a", right).

The morphological changes are evident from the optical properties of AuNC, as observed by the naked eye (Figure 1a) and by the UV-vis absorption spectroscopy of the Au colloid at 0 and 7 days after LI (Figure 2a). In the spectrum of pristine Au nanospheres, the typical SPR band at 520 nm is clearly visible, whereas no absorption is measured in the red and NIR part of the spectrum. After LI, the SPR band is sensibly damped indicating that size reduction of nanospheres occurred. In fact, when nanoparticles size decreases to few nanometers, an additional relevant contribution to conduction electron relaxation frequency appears, due to the electron scattering at particles surface, with the consequent flattening of the SPR band.[7, 8, 40, 41] Remarkably, the absorbance in the red and NIR increased soon after laser treatment (0 days after LI), suggesting the formation of elongated

nanostructures in which new longitudinal plasmon modes are possible at frequencies red shifted compared to gold nanospheres. In AuNC aged for 7 days, plasmon absorbance further grows generating a flat and broadband spectrum from the visible to the infrared.

To further substantiate the above observations, we used the discrete dipole approximation (DDA) method to model the optical properties of AuNC. DDA allows the calculation of optical properties for objects with any shape, included asymmetric AuNC, by dividing their solid volume in an array of dipoles arranged in a cubic lattice.[5, 8, 42, 43] The extinction cross section (σ_{Ext}) was calculated for 15 distinct AuNC taken from three randomly selected regions of a TEM picture (see Figure 2b). The results show that AuNC have multiple plasmon modes ranging from the visible to the NIR, as a consequence of their asymmetric coral-like shape. The DDA results also provide further evidence that particles with the largest aspect ratio have intense plasmon absorption at red and NIR frequencies (see Figure 2b). Overall, although each AuNC has a characteristic SPR profile, the convolution of all the SPR gives a broadband plasmon band from the visible to the NIR (Figure 2b), providing an explanation to the black color experimentally observed. This explains why AuNC dispersions have "flat" plasmon absorption instead of a single band in the red-NIR such as that originated by longitudinal plasmon excitation in Au nanorods with well defined aspect ratio.[6, 9]

Importantly, from DDA calculations in all the AuNC considered, we found that the absorption cross section is 200 times larger than the scattering cross section, as expected for gold nanostructures with size of only few nanometers. Therefore, we performed resonant light scattering measurements to experimentally assess the absence of scattering in AuNC aqueous dispersions (Figure 2c). For sake of comparison, a "positive control" consisting in a sample of commercial 60 nm spherical Au nanoparticles was also considered, for which theory predicts a scattering contribution comparable to absorption.[7, 40, 44] With our measurements, light scattering was observed only with the 60 nm AuNPs, while AuNC gave no signal in the whole spectral range allowed by the instrument. Therefore, numerical calculations and experimental results showed that AuNC are pure plasmon absorbers with broadband response from the visible to the NIR. These features meet the main requirements recently identified for the optimal application in areas such as photothermal therapy[9] or photothermal imaging.[45]

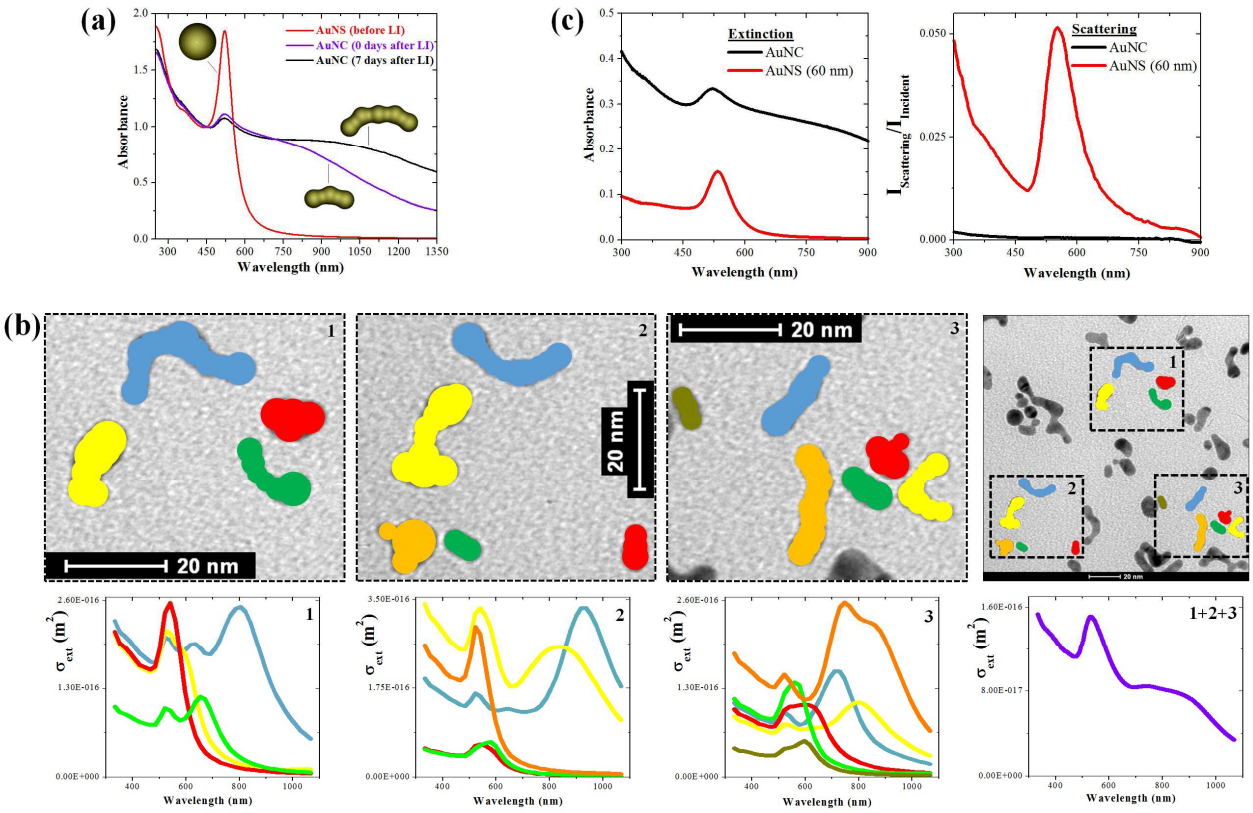

Figure 2. a) UV-vis absorption spectra of the AuNS before LI and of AuNC at 0 and 7 days after LI. b) DDA calculations of the orientationally averaged extinction cross section for 15 AuNC randomly selected from TEM images of the AuNC sample 0 days after LI. c) Absorbance (left) and scattering (right) of AuNC and commercial AuNS (60 nm) dispersions in water.

The refinement of synthesis parameters is important for the formation of AuNC and the appearance of a broadband plasmon absorption. In particular, a positive effect is obtained by increasing the laser pulses fluence and the fraction of ethanol in the liquid mixture. These results are shown in Figure 3a-b, where we plotted the integral of the absorbance from 460 to 1300 nm for AuNC dispersions at 0 days after LI, normalized to the same integral for the starting AuNS dispersion. Nonetheless, the largest absorption improvement is observed by ageing the irradiated solution on a time scale of days, as shown in Figure 3c where the optical properties were monitored at 0, 1, 3, 7, 14, 21, 28, 35, 42, 49 and 56 days after LI. The absorbance in the 460 – 1300 nm spectral region experienced a sensible increase in the first days after LI, reaching a plateau after the 7th day. It should be noted that, prior to UV-vis spectra, each aliquot taken from the aged AuNC batch was incubated with a large excess of thiolated PEG (5000 Da), dialysied and redispersed in pure water. This procedure was necessary to disperse AuNC in water by binding with the thiol group of the hydrophilic polymer, thus excluding the contribution of reversible particles aggregation as a possible source of the NIR absorption.

Ageing experiments suggest that the broadband plasmon absorption derives from the anysotropic particles growth along one preferential direction, i.e. by unidirectional coalescence and soldering of photofragmented Au nanoparticles on a time scale of days. AuNC morphology and the electronic contrast observed with TEM both support this observation, since the elongated gold structures appear as being composed of a linear assembly of smaller spherical or spheroidal nanoparticles, which in most cases are well recognizable even after interparticle soldering into a whole metal nanocoral (see Figure 3d). Consequently, the formation of AuNC is not a direct morphological effect of LI, i.e. of a one step laser reshaping mechanism. This hypothesis was further assessed by performing LI of AuNS dispersed in a solution containing an excess of thiolated PEG. The polymer in excess had the function of coating particles surface before and after the photofragmentation, to prevent coalescence at longer times and preserving the shape of Au nanocrystals just after the interaction with laser pulses. With this experiment, we clearly observed particles photofragmentation by the damping of the SPR (Figure 3e), but we did not observe the increase of plasmon absorption in the red and NIR, and plasmon properties remained unchanged also at longer times. This clearly showed that laser pulses have the role of producing a large number of small Au nanoparticles by photofragmentation, whereas coalescence and unidirectional growth occurs on a longer time scale.

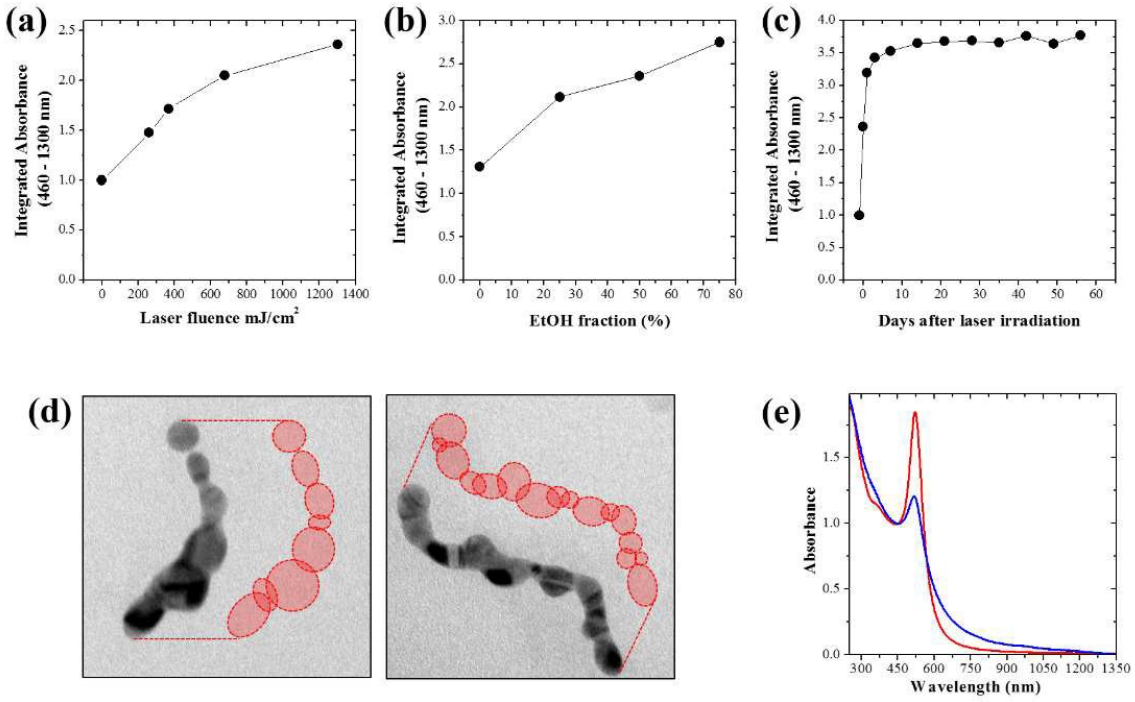

Figure 3. Plot of the integrated absorbance of AuNC samples at 0 days after LI, obtained with different laser fluence (a) and ethanol fraction in the starting solution (b). The absorbance was integrated in the 460 – 1300 nm range and normalized to the same integral measured on the starting AuNS solution before LI. c) Plot of the integrated absorbance at different days after LI. d) The morphology and the electronic contrast observed with TEM analysis of AuNC both suggest that nanocorals form by soldering of smaller spheroidal Au nanoparticles (the recongizable "monomers" are sketched with red circles in the figure) along anisotropic directions. e) UV-vis spectra before (red line) and after (blue line) LI of a AuNS solution containing an excess of thiolated PEG. In this case, only size reduction of AuNS, without broadband absorbance increment, is observed.

The formation of AuNC with broadband plasmon absorption occurs without chemicals, surfactants or templating molecules adsorbed on particles surface, hence the operator is free to decide the preferred ligand among all those capable of coating the surface of Au nanostructures, such as thiols or ionic polymers. In the present case, we coated AuNC with thiolated PEG to achieve stability in aqueous phase and in organic solvents such as CH_2Cl_2. The coating of AuNC with PEG was confirmed by FTIR spectroscopy on the dried particles (Figure 4a), other than being clearly appreciable by the stability of nanoparticles during the multiple dialysis and washing steps before the spectrophotometric analysis. Importantly, PEG-AuNC were easily dried and redispersed in water or in CH_2Cl_2 (Figure 4b), and were included in hydrophilic or hydrophobic polymeric matrixes such as PVA, PMMA and PS (Figure 4c). In general, such a versatility allows a practical way to store AuNC as a dried powder before use.

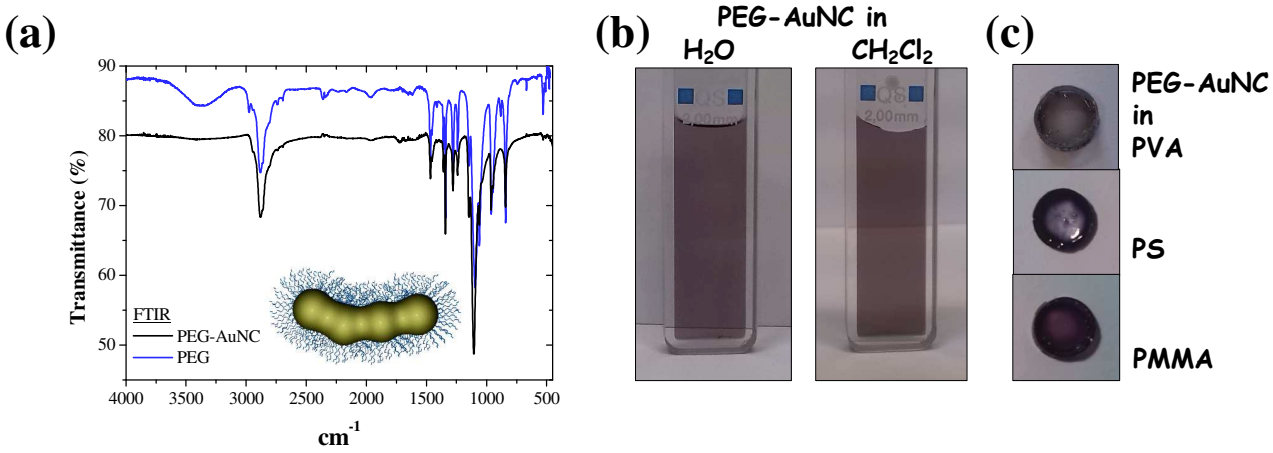

Figure 4. a) FTIR spectra of PEG-AuNC as a dried powder (black line) and of a reference PEG sample. b) PEG-AuNC powder re-dispersed in water and in CH_2Cl_2. c) Polymeric nanocomposites containing PEG-AuNC embedded in PVA, PS and PMMA matrixes.

Given the broadband plasmon absorption and the pure absorption features, we tested the photothermal properties of AuNC in water solution and in different polymeric matrixes. The AuNC dispersion in water (1.6 mM in Au atoms) was irradiated with continuous wave laser lines at various wavelengths ranging from the visible to the NIR (568, 647, 700, 800, 900 and 1000 nm), all with the same intensity of 1.27 W/cm^2. Thermal imaging of the quartz cuvette containing the samples showed the rapid heating of the AuNC solution at all wavelengths considered (Figure 5a). Temperature increments of ca. 15 °C were observed in all cases, and we measured unitary efficiency of light-to-heat conversion in all cases, by fitting temperature profiles with the exponential models proposed by Govorov and co.[46]. Importantly, AuNC showed excellent photothermal stability for the whole duration of the experiment (i.e. for several hours), without any change in the light-to-heat conversion efficiency of nanoparticles.

When AuNC are included in the polymeric matrixes, the heating ability is sensibly increased by the lower heat dissipation rate of the solid phase compared to the liquid solution (see Figure 5b), in fact temperature increments up to 90°C were measured by irradiation at 785 nm for 10 minutes with a fluence of 1.12 W/cm^2.

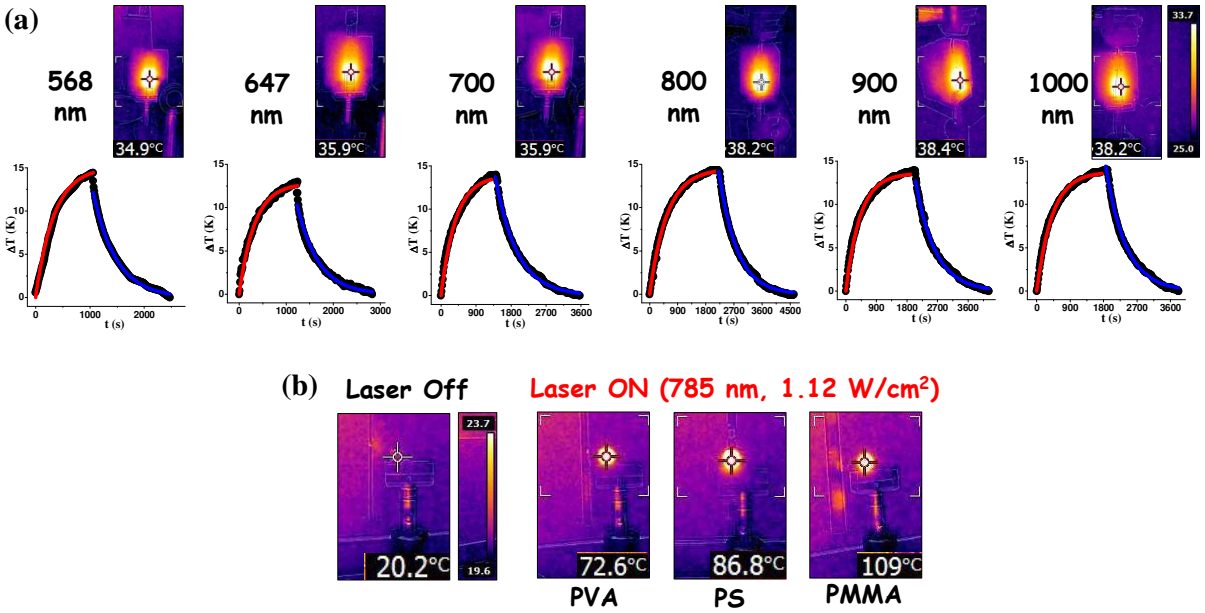

Figure 5. a) Thermal imaging and temperature profiles of AuNC aqueous solution in a quartz cuvette, irradiated with cw laser lines from the visibile to NIR. Heating and cooling profiles were fitted with exponential models (red and blue lines respectively). b) Thermal imaging of polymeric AuNC nanocomposites before (left) and after (right) 785 nm laser irradiation.

In consideration of the phohothermal properties in the red and NIR and the dispersibility in aqueous environment, PEG-AuNC are of interest for nanobiotechnological applications such as photothermal therapy of cancer, photoacoustic imaging or photothermal antimicrobial activity. Therefore, we performed *in vitro* biocompatibility studies to obtain experimental evidences about AuNC's safe-by-design and their suitability for bio-applications. Since cytotoxicity may be dependent on the cell type,[47] we evaluated cell viability by incubating PEG-AuNC with one primary cell type, i.e. human fibroblasts, and three tumor cells lines, i.e. HeLa, PC-3 and CAPAN-1 (Figure 6). The results were compared with PEG-AuNS, which are recognized for their biocompatibility also at doses as high as 60 μg/mL.[33] In all cases, no toxicity was observed after 24 hours of incubation with either AuNC or AuNS. Moreover, we excluded the activation of early apoptosis events in cells by measuring the externalization of phosphatidylserine by Annexin V staining after 24 hours of incubation with AuNC (see Table 1).

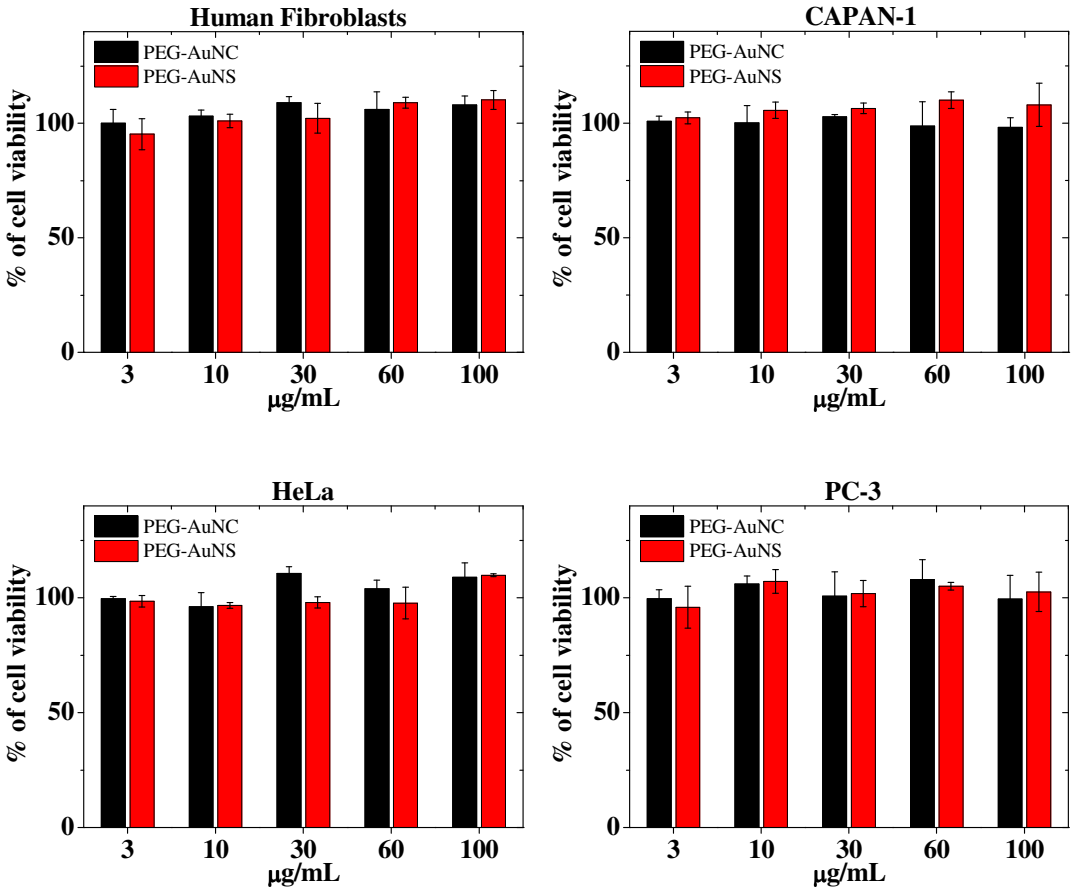

Figure 6. Cell viability experiments performed on human fibroblasts, CAPAN-1, HeLa and PC-3 cells incubated for 24 hours with PEG-AuNC or PEG-AuNS at concentration variable from 3 to 100 µg/mL.

Cells type	Untreated	AuNC treated	Positive Control Sample
HeLa	0.4 %	0.5 %	0.9 % (*)
PC-3	0.5 %	0.6 %	8.1 % (*)
CAPAN-1	0.5 %	0.7 %	13.1 % (*)
Human Fibroblasts	0.6 %	0.8 %	5.5 % (**)

Table 1. Percentage of apoptosis after 24 hours incubation with AuNC (at 60 µg/mL). (*) Positive control samples were starved 48 hours with a low percentage of FBS (0.5%). (**) Positive control sample was treated 24 hours at 37°C with anti-CD44 antibody.

Discussion

AuNC with broadband plasmon absorption were obtained by 532 nm LI and ageing of AuNS dispersed in water/ethanol solution. Safe-by-design and environmentally friendly synthetic approaches are stringent requirements for the synthesis of nanomaterials aimed at exploitation in real-life technology.[33, 48-50] The LI is performed under continuous flow using only class 3 solvents,

and this is an important advantage for nanomaterials synthesis scale up.[48, 49, 51] Besides we successfully assessed *in vitro* the suitability of AuNC for biological applications.

Biocompatibility of AuNC is the consequence of the synthetic protocol which starts from pure gold nanostructures obtained in the absence of undesired chemicals.[33] Standard methods to obtain anisotropic gold nanoparticles in solution consist in chemical reduction of metal salts in the presence of stabilizing molecules and, although a large number of variants have been developed, often reducing agents, complexing molecules and stabilizing agents such as CTAB are required.[33] Indeed, although the biosafety of Au nanoparticles is well known from literature and their medical usage in the human body has been approved by the FDA,[10, 26] a frequent issue with plasmonic nanoparticles absorbing in the NIR is the presence of synthesis byproducts affecting their biocompatibility, such as CTAB.[33, 50] The biocompatibility problem can be solved by a ligand exchange process,[39] which usually requires two or more steps and a fine control of several parameters such as the concentration of coating agents, the type of solvents, the temperature and the reaction time to prevent the destabilization of the colloidal systems.[37-39] In our case, we used laser assisted synthesis to obtain pristine AuNS and to transform them into AuNC by a "green" protocol which avoids the use of chemicals. In addition, the AuNC transversal size below 10 nm is compatible with the shape requirements for in vivo applications and body disposal.[50, 52, 53] For instance, elongated nanostructures such as gold nanorods and carbon nanotubes can be excreted by kidneys when their transversal size is lower than glomerular pore size, which is of the order of 10 - 5 nm.[50, 52] Clearance of inorganic non-toxic nanomaterials may take place also by epatobiliar excretion from liver to the intestine, with higher efficiency for smaller objects.[50, 52] Therefore, due to their inherently low toxicity and small size, AuNC open several opportunities for nanomedicine applications.

Experiments showed that the aspect ratio of AuNC increases with time after laser treatment, with a parallel improvement of the red and NIR absorption. Conversely, when stabilizers such as thiolated PEG are present, the formation of AuNC is inhibited. This is a clear indication that AuNC formation mechanism takes place in two stages: photofragmentation and anisotropic regrowth (Figure 7). On the other hand, the synthetic procedure does not require chemicals or templating agents to direct particles growth along specific crystallographic directions.

Laser induced fragmentation of AuNS takes place by surface evaporation and Coulomb explosion.[54-57] Surface evaporation occurs when nanoparticles temperature exceeds the boiling temperature at the environment pressure, which can be much higher than room pressure because of the simultaneous solvent heating and vaporization around the absorbing object.[54, 55] Vaporization alone yields to a layer-by-layer size reduction process and is usually compatible with a bimodal size

distribution of nanoparticles, unless the laser fluence is high enough to originate also Coulomb explosion.[54, 58] Coulomb explosion occurs when a large number of electrons are ejected, generating a multiply ionized nanoparticle that undergo spontaneous fission because of the charge repulsion.[54, 56, 59] Coulomb explosion is possible by thermoionic electron emission because, at temperatures of thousands of K, the most energetic electrons in the tail of the Fermi distribution overcome the work function of the metal and escape from particles surface.[54, 56, 59] At the fluence of 1300 mJ/cm^2 used in the present work, both mechanisms take place simultaneously, yielding small Au nanoparticles.[54, 58]

We experimentally demonstrated that photofragmentation does not lead directly to the formation of AuNC, since LI of AuNS in the presence of excess thiolated PEG gave smaller AuNS (see Figure 3e). Instead, AuNC forms after photofragmentation, by unidirectional coalescence and reorganization of Au fragments. The template-free one-dimensional assembly of nanoparticles has been widely observed experimentally in nanocolloids of metals, metal oxides, and semiconductors, and these anisotropic nanoparticle arrays are of particular interest in photonics, nanoelectronics, optoelectronics, nanomagnetism, and biosensor devices.[12, 15, 60, 61] However, a satisfactory quantitative description of their formation mechanism is lacking at the moment, and only few recent reports considered Brownian dynamics simulations to model the aggregation of nanoparticles in liquid environment.[15, 60, 61] In these studies, the interaction between particles is described within the framework of the Derjaguin, Landau, Verwey, Overbeek (DLVO) theory, by adopting a sum of steric repulsion, screened Coulomb repulsion potential, dispersive van der Waals attraction and electrostatic dipolar attractive interactions (the latter only in the case that permanent electrostatic dipoles are present in nanoparticles).[15, 60, 61] These studies showed that unidirectional nanocrystals assembly arise from random collisions of nanoparticles diffusing in the liquid medium.[15, 60, 61] In particular, the spontaneous formation of nanoparticle chains occurs by diffusion-limited aggregation, but only when the rearrangement of the chain monomer into a more compact structure is hindered by irreversible attractive forces after collision.[15, 60, 61] According to numerical simulations, the typical time scale for the growth of linear assemblies depends on the probability of sticking after collision and by the number of collisions in the system,[15, 60, 61] explaining why growth proceeds for days or even weeks as observed in this work.

A key point emerging from numerical simulations is that the resultant DLVO potential energy is isotropic for isolated nanoparticles but it becomes anisotropic in a dimer of particles.[12, 60, 61] Hence, when a third nanoparticle approaches a dimer, the anisotropic repulsive potential offers conical spaces with lower resistance to nanoparticle attachment at the two ends of the dimer.[15, 60, 61] In this way, the formation of a linear trimer is favoured over a more compact structure, and growth proceeds in analogous way for all the other nanoparticles approaching the chain.[12, 15, 60, 61]

According to this mechanism, elongated nanoparticles "catalyzes" the formation of AuNC with increasing aspect ratio by addition of one photofragmented Au particle at time or by coalescence of two smaller chains to yield a single longer AuNC.

All simulations pointed to the necessity for a strong sticking interaction between particles as a prerequisite to maintain the linear assembly.[12, 15, 60, 61] In the simplified case of a generic particle *"a"* which collides with a second set of particles "*b"*, the bimolecular sticking frequency (F_{ab}) is given by:[62]

$$F_{ab} = \gamma_{ab}\pi N_A (d_a + d_b)(s_a + s_b)\frac{k_B T}{\eta} c_b \qquad (1)$$

where d_a and d_b are particles size, γ_{ab} is the sticking coefficient (i.e. the probability that cluster b sticks to a after collision), N_A is the Avogadro number, s_a and s_b are geometrical factors related to particles shape (for spherical particles $s^{-1}=3\pi d$), k_B is the Boltzmann constant, η is the solution viscosity, T is the system temperature and c_b is the concentration of b species. Given the almost exponential dependence of η on T, the temperature dependence of F_{ab} can be approximated as $\sim Te^{-kost/T}$.

In our synthetic approach γ_{ab} is large because AuNS are obtained by LASiS in water without any stabilizer or coating agent, and no reducing agents or templating molecules are present in the whole process,[40, 58, 63] therefore the surface of photofragmented nanoparticles is available for the establishment of a strong sticking interaction after collision. In our experiments, AuNC remained unperturbed after the addition of thiolated PEG, and TEM analysis clearly showed that they are fromed by a unique continuous nanostructure, instead of aggregates of distinct nanoparticles. Therefore, coalescence of photofragmented Au nanocrystals is followed by a nanosoldering process, which is possible for the large surface energy of Au atoms in nanoparticles with small curvature radii and without capping agents.[64-68] It has been reported also that Au atoms and small clusters form during photofragmentation of Au nanoparticles in liquid phase.[54-56] These species can survive for times of the order of 100 μs in aqueous solutions and may originate high mobility adsorbates on the surface of AuNC soon after LI.[54, 69]

Photofragmentation of Au nanospheres contributes to F_{ab} also by increasing the concentration of Au particles and solution temperature.[54, 56, 65]

The addition of ethanol to the aqueous dispersion of AuNS before LI has the effect of decreasing the viscosity η with a consequent increase of F_{ab}. Besides, the addition of organic solvents to aqueous colloidal dispersions of charged Au nanoparticles is generally associated to the destabilization of the system by decreasing the electrostatic repulsive potential.[12, 70, 71] Sometimes this is attributed to the lower medium dielectric constant.[12, 70, 71] However, the energy barrier that

must be overcome for sticking of two nanoparticles after collision is increased by decreasing the medium dielectric constant according to the Yukawa potential V_Y, which describes the electrostatic repulsion between charged particles:[15]

$$V_Y = \frac{q_e^{\,2} e^{-\kappa x}}{4\pi\varepsilon_0\varepsilon_s x}\left(\frac{Z_{eff} e^{-\kappa R}}{1+\kappa R}\right)^2$$

where x is the distance between particles of radius R and effective charge Z_{eff}, q_e is the electron charge, ε_0 and ε_s are vacuum and solvent dielectric constants, and κ^{-1} is the Debye length

$$\kappa^{-1} = \left(\frac{k_B T \varepsilon_0 \varepsilon_s}{2\rho q_e^{\,2} z^2}\right)^{1/2}$$

with k_B the Boltzmann constant and ρ the density of electrolytes with average charge z.

Therefore, one can exclude that the energy barrier for particles assembly is reduced after addition of ethanol as an effect of the lower dielectric constant of the 1:1vol mixture with water. Conversely, the stability of the colloidal suspension depends on the presence of surface electric charges,[12, 15, 72] quantitatively espressed by the dependence of the Yukawa potential on Z_{eff}. Indeed, it is well known that low-dielectric-constant media have a low degree of electrolyte dissociation compared to water,[73, 74] with consequent decrease of Z_{eff}. In the specific case of Au nanoparticles generated by LASiS in 10^{-5} M aqueous solutions of NaCl, 3-6% of surface gold atoms are oxidized to AuOH, and there is an equilibrium between the neutral (AuOH) and the negatively charged (AuO^-) species.[75, 76] This suggests that ethanol increases the proportion of the undissociated AuOH surface groups, corresponding to the decrease of Z_{eff}. We experimentally verified this hypothesis by ζ-spectroscopy measurements (see Figure 8), and we found that AuNS electrostatic repulsive potential drops from -38 mV to -11 mV after addition of ethanol, while remaining at comparable values after laser irradiation (-15 and -8 mV for AuNC at, respectively, 0 and 7 days after LI). These findings well agrees with the observation of Au nanowire formation during LASiS in organic solvents, supercritical fluids and superfluid He, were the double layer colloidal repulsive potential is inhibited.[14, 77, 78]

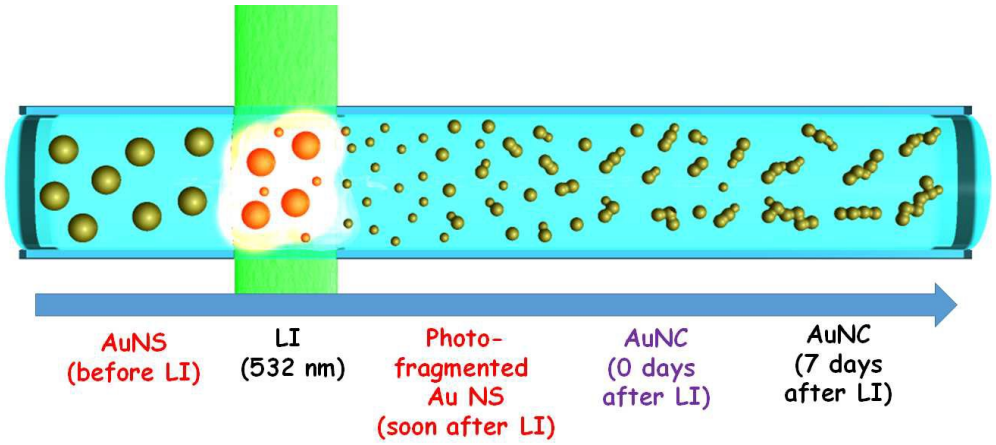

Figure 7. Sketch of AuNC synthesis: AuNS in water/ethanol mixture are irradiated with 532 nm (9 ns) laser pulses. After photofragmentation, Au nanocrystals undergo to a process of agglomeration and anisotropic growth to yield AuNC. The AuNC formation is more rapid at high temperature, low viscosity and high nanoparticles concentration occurring just after absorption of laser pulses, and prosecute on a time scale of days after the LI process. The smallest Au nanocrystal aggregates (i.e. dimers and trimers) have an anisotropic electrostatic repulsive potential, which favours the growth along the extremity of the nanostructure forming elongated AuNC. See discussion for further details.

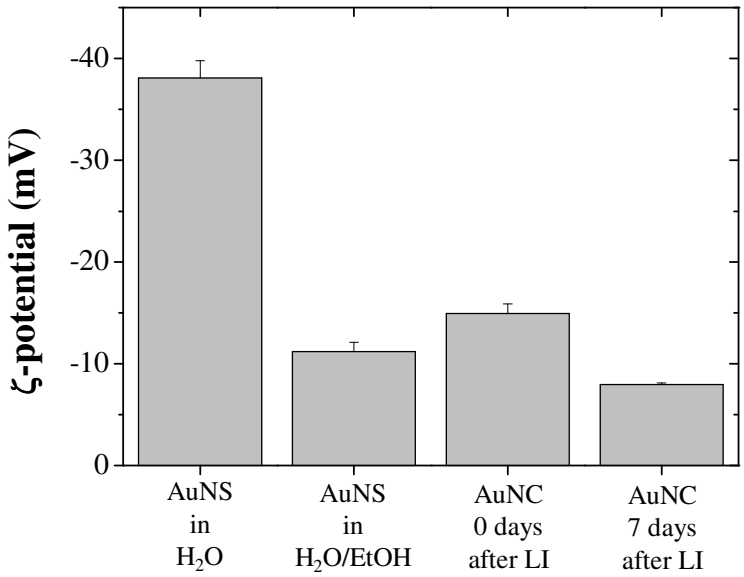

Figure 8. ζ-spectroscopy measurements of AuNS dispersed in water or in water:ethanol 1:1, and on AuNC at 0 and 7 days after LI.

Conclusion

We described the laser assisted synthesis of AuNC endowed with broadband plasmon absorption from the visible to the NIR. AuNC formation is initiated by photofragmentation of spherical AuNPs dispersed in water/ethanol solution, previously obtained by laser ablation in water without

chemicals or stabilizers. Then, the nanoparticles spontaneously prosecute their unidirectional growth in solution, as a consequence of the balance between the electrostatic repulsion force and the attractive dipolar interactions in the colloidal system. The laser assisted approach introduces several benefits in the achievement of broadband plasmon absorbers such as the synthesis under continuous flow, the environmentally friendly procedure without chemicals, stabilizers or templating molecules, the biocompatibility and the easy surface functionalization of products.

AuNC shape and the small size makes them pure absorbers exploitable for the efficient photothermal applications in the visible and NIR range. The one step easy surface conjugation with biopolymers, the photothermal efficacy in the visible-NIR range and the absence of cytotoxicity of AuNC were assessed experimentally. Overall, results suggest that our safe-by-designed AuNC are eligible candidates for multiple photothermal applications.

Methods

Synthesis of AuNC.

Pristine AuNS were obtained by laser ablation synthesis in solution (LASiS) according to a well established protocol.[40, 58, 63, 79] Briefly, 1064 nm (5 ns, 50 Hz) laser pulses were focused on a 99.99% pure Au plate dipped in distilled water containing NaCl 10^{-5}M. For LI experiments, AuNS were mixed 1:1 with HPLC grade ethanol (from Sigma Aldrich) at 1 mM final concentration of Au atoms. The mixture was fluxed through a glass channel (diameter of 1.8 mm) at a velocity of 0.2 mL/minute. Laser pulses at 532 nm (10 ns, 10 Hz) were focused with a f:350mm lens on the glass channel at a final fluence of 1300 mJ/cm^2.

Surface functionalization was performed by adding thiolated polyethylene glycol (PEG, 5000 Da, from Lysan Bio) to the NC solution. After sonication with a bath sonicator Branson CPXH for 60 minutes, the excess PEG was removed by dialysis with Sartorius Vivaspin concentration membranes (10 kDa) at 5000 rcf and then washed several times with distilled water.

To obtain polymer-AuNC nanocomposites, we first mixed the solution of PEG-coated NC with a liquid solution containing the polymer. We used polymethylmethacrylate (PMMA, 120 kDa, from Sigma-Aldrich) and polystyrene (PS, 192 kDa, from Sigma-Aldrich) dissolved in CH_2Cl_2 at 200 mg/mL, or polyvinyl alcohol (PVA, 200 kDa, from Fluka) dissolved in distilled water at 50 mg/mL. For the inclusion in PMMA and PS, the AuNC aqueous solution was first dried with a rotavapor and then the nanoparticles were redissolved in CH_2Cl_2. The polymer-NC mixtures were poured into a mold and the solvent removed at room temperature (for CH_2Cl_2 solutions) or at 40°C (for aqueous solutions).

Characterization of AuNC.

UV-visible-NIR spectroscopy was performed with a Varian Cary 5 spectrometer using 2 mm optical path quartz cells. The concentration of Au atoms in each solution was evaluated by optical absorption spectroscopy according to previously published protocols.[5, 80] TEM analysis was performed with a FEI Tecnai G2 12 operating at 100 kV and equipped with a TVIPS CCD camera. Samples were prepared by evaporating AuNC suspensions on a copper grid coated with an amorphous carbon holey film. Statistics considered more than 300 nanoparticles for each sample, using the ImageJ software. Resonant light scattering analysis was performed with a Varian Cary Eclipse fluorescence spectrophotometer in 1 cm optical path fluorescence quartz cells, using the synchronous scan modality. FTIR measurements were performed with a Perkin Elmer 1720X spectrometer. Samples were obtained by evaporating the solvent and deposing the AuNC powder on a KBr substrate. ζ-spectroscopy was performed with a Malvern Zetasizer Nano ZS in DTS1070 cells.

For 0 days after laser irradiation, we mean a time between 0.5 and 6 hours, which is the typical time elapsed between the LI process and the post-irradiation manipulation of the sample for further analysis such as UV-visible-NIR spectroscopy, TEM sample deposition, etc.

Numerical calculations.

Optical properties of AuNC were calculated by the Discrete Dipole Approximation (DDA) method using the software developed by Draine and Flatau (DDSCAT 7.1 and the relative DDFIELD code).[42] We used a number of dipoles of 10^5 for each target, corresponding to a maximum interdipole spacing of 0.1 nm. For metal particles in the 2 – 200 nm size range, an error smaller than 10% is usually achieved using a number of dipoles at least of the order of 10^4 and using interdipole spacing much smaller than the wavelengths of interest.[5, 42, 43] The average over 27 different orientations was considered for the computation of the extinction, absorption and scattering cross sections of each object. The refractive index of water and the size corrected dielectric constant for Au, as reported in ref.[5, 7, 40], were used.

Photothermal heating.

Photothermal heating experiments were carried out at 568 nm and 647 nm with a Coherent Innova 70 Argon/Krypton continuous wave laser, and at 700 nm, 800 nm, 900 nm and 1000 nm with a Spectra-Physics 3900s Titanium/Sapphire continuous wave tunable laser pumped by a Coherent Verdi G7 OPSL laser. Laser power was set to 250 mW for each wavelength and the laser spot was 5 mm in diameter (1.27 W/cm^2). Polymeric nanocomposites were irradiated at 785nm with a

Renishaw solid state laser model HPNIR (220 mW, 5 mm spot size, 1.12 W/cm^2). A thermal camera model FLIR E5 was used to capture the calibrated digital thermographic infrared images of heated samples. Temperature in the liquid samples was monitored also with a K-type thermocouple dipped in a dark region of the cuvette. Fit of the heating (laser light on) and cooling (laser light off) curves was performed with single-exponential laws according to the models described by Govorov and co. in ref.[46].

Cell culture, cytotoxicity and apoptosis assays.

HeLa (human cervical cancer cells), PC-3 (human prostate tumor cells), CAPAN-1 (human pancreatic tumor cells) and human fibroblasts were obtained from American Type Culture Collection (ATCC, Rockville, USA). The cells were maintained at 37°C in a humidified atmosphere containing 5% CO_2 and 90% of humidity; HeLa, PC-3 and CAPAN-1 cells were cultured in RPMI 1640 Medium and supplemented with 2 mM L-Glutamine and 0.01 M HEPES. Human fibroblasts were cultured in Dulbecco Modified Eagle's Medium (DMEM) containing 3.7 g/L sodium bicarbonate, 4.5 g/L glucose and supplemented with Glutamine and HEPES. Moreover all the media were supplemented with 10% heat-inactivated foetal bovine serum (FBS) (Invitrogen, NY, USA) and antibiotics (0.1 mg/mL streptomycin and 100 units/mL penicillin G (Sigma-Aldrich, St Louis, MO, USA).

For the viability assays cells were seeded, one day before the assay, at an appropriate cell density in 90 µl of complete medium in 96 well culture microplates; the day after, the cells were incubated in triplicate with 10 µl of either PEG-AuNC or the control PEG-AuNS. After 24 hours, the cells were washed and incubated in the medium supplemented with XTT reagent (Sigma-Aldrich, St Louis, MO, USA), according to the supplier instructions; cell viability was measured at 450 nm by a microplate reader. The percent of cell viability was estimated analyzing the values obtained from treated cells with respect to mock treated cells.

To evaluate the early apoptosis event of the phosphatidylserine externalization, cells were seeded in 12 well culture plates, on day before, at an appropiate cell density; then they were treated for 24 hours at 37 °C with AuNC at a concentration of 60 µg/mL. At the end of the incubation cells were detached, washed and stained with Annexin V-FITC reagent. Fluorescence was acquired by a BD FACSCanto^{TM} II (Becton Dickinson, San Jose, California, USA) flow cytometer and analyzed with the FACSDiva Software. As positive control of apoptosis HeLa, PC-3 and CAPAN-1 cells were starved 48 hours with a low FBS concentration (0.5 %); conversely human fibroblasts were treated 24 hours with an anti-CD44 antibody at 20 µg/mL.

Acknowledgments.

Prof. M. Meneghetti is gratefully acknowledged for useful discussions. Financial support from University of Padova (PRAT no. CPDA114097/11 and Progetto Strategico STPD11RYPT_001) and MIUR (PRIN MULTINANOITA no. 2010JMAZML_001) is gratefully acknowledged.

Bibliography

1) S. Eustis and M. A. El-Sayed, *Chem. Soc. Rev.,* 2006, **35**, 209-217.

2) M. C. Daniel and D. Astruc, *Chem. Rev.,* 2004, **104**, 293-346.

3) R. A. Sperling, P. R. Gil, F. Zhang, M. Zanella and W. J. Parak, *Chem. Soc. Rev.,* 2008, **37**, 1896-1908.

4) P. K. Jain, X. Huang, I. H. El-Sayed and M. A. El-Sayed, *Plasmonics,* 2007, **2**, 107-118.

5) V. Amendola, O. M. Bakr and F. Stellacci, *Plasmonics,* 2010, **5**, 85-97.

6) N. Harris, M. J. Ford, P. Mulvaney and M. B. Cortie, *Gold Bull.,* 2008, **41**, 5-14.

7) U. Kreibig and M. Vollmer, *Optical Properties of Metal Clusters*, Springer, Berlin, 1995.

8) K. L. Kelly, E. Coronado, L. L. Zhao and G. C. Schatz, *J. Phys. Chem. B,* 2003, **107**, 668–677.

9) M. A. Mackey, M. R. Ali, L. A. Austin, R. D. Near and M. A. El-Sayed, *J. Phys. Chem. B,* 2014, **118**, 1319-1326.

10) X. Huang, P. K. Jain, I. H. El-Sayed and M. A. El-Sayed, *Photochem. Photobiol.,* 2006, **82**, 412-417.

11) A. Teulle, M. Bosman, C. Girard, K. L. Gurunatha, M. Li, S. Mann and E. Dujardin, *Nat. Mater.,* 2014, .

12) L. J. Hill, N. Pinna, K. Char and J. Pyun, *Prog. Polym. Sci.,* 2015, **40**, 85-120.

13) L. O. Herrmann, V. K. Valev, C. Tserkezis, J. S. Barnard, S. Kasera, O. A. Scherman, J. Aizpurua and J. J. Baumberg, *Nat. Commun.,* 2014, **5**.

14) L. D'Urso, G. Grasso, E. Messina, C. Bongiorno, V. Scuderi, S. Scalese, O. Puglisi, G. Spoto and G. Compagnini, *J. Phys. Chem. C,* 2009, **114**, 907-915.

15) J. Richardi, *J. Chem. Phys.,* 2009, **130**, 044701.

16) V. Amendola, R. Sajia, O. M. Maragò and A. Iatì, *Nanoscale,* 2015, .

17) O. Neumann, C. Feronti, A. D. Neumann, A. Dong, K. Schell, B. Lu, E. Kim, M. Quinn, S. Thompson, N. Grady, P. Nordlander, M. Oden and N. J. Halas, *Proc. Natl. Acad. Sci. U. S. A.,* 2013, **110**, 11677-11681.

18) M. Salmistraro, A. Schwartzberg, W. Bao, L. E. Depero, A. Weber-Bargioni, S. Cabrini and I. Alessandri, *Small,* 2013, **9**, 3301-3307.

19) K. Ueno, S. Juodkazis, T. Shibuya, Y. Yokota, V. Mizeikis, K. Sasaki and H. Misawa, *J. Am. Chem. Soc.,* 2008, **130**, 6928-6929.

20) K. Turcheniuk, C. Hage, J. Spadavecchia, A. Y. Serrano, I. Larroulet, A. Pesquera, A. Zurutuza, M. G. Pisfil, L. Héliot and J. Boukaert, *J. Mater. Chem. B,* 2015, **3**, 375-386.

21) C. Hsiao, H. Chen, Z. Liao, R. Sureshbabu, H. Hsiao, S. Lin, Y. Chang and H. Sung, *Adv. Funct. Mater.,* 2014, **25**, 721.

22) H. Aoki, M. Nojiri, R. Mukai and S. Ito, *Nanoscale,* 2015, **7**, 337-343.

23) A. Taruttis and V. Ntziachristos, *Nat. Photon.,* 2015, **9**, 219-227.

24) Y. Xu, R. He, D. Lin, M. Ji and J. Chen, *Nanoscale,* 2015, .

25) S. R. Abulateefeh, S. G. Spain, J. W. Aylott, W. C. Chan, M. C. Garnett and C. Alexander, *Macrom. Biosci.,* 2011, **11**, 1722-1734.

26) X. Huang, I. H. El Sayed, W. Qian and M. A. El Sayed, *J. Am. Chem. Soc.,* 2006, **128**, 2115-2120.

27) E. B. Dickerson, E. C. Dreaden, X. Huang, I. H. El Sayed, H. Chu, S. Pushpanketh, J. F. McDonald and M. A. El Sayed, *Cancer Lett.,* 2008, **269**, 57-66.

28) W. Li, U. Guler, N. Kinsey, G. V. Naik, A. Boltasseva, J. Guan, V. M. Shalaev and A. V. Kildishev, *Adv. Mater.,* 2014, **26**, 7959-7965.

29) P. Nikolaou, C. Mina, M. Constantinou, L. Koutsokeras, G. Constantinides, E. Lidorikis, A. Avgeropoulos, P. Kelires and P. Patsalas, *Thin Solid Films,* 2014, .

30) F. Ratto, E. Witort, F. Tatini, S. Centi, L. Lazzeri, F. Carta, M. Lulli, D. Vullo, F. Fusi and C. T. Supuran, *Adv. Funct. Mater.,* 2015, **25**, 316-323.

31) S. Son, J. Nam, J. Kim, S. Kim and W. J. Kim, *ACS nano,* 2014, **8**, 5574-5584.

32) Y. Liu, X. Han, L. He and Y. Yin, *Angew. Chem. Int. Ed.,* 2012, **51**, 6373-6377.

33) A. M. Alkilany and C. J. Murphy, *J. Nanop. Res.,* 2010, **12**, 2313-2333.

34) C. Singh, Y. Hu, B. P. Khanal, E. R. Zubarev, F. Stellacci and S. C. Glotzer, *Nanoscale,* 2011, **3**, 3244-3250.

35) E. E. Connor, J. Mwamuka, A. Gole, C. J. Murphy and M. D. Wyatt, *Small,* 2005, **1**, 325-327.

36) C. Kinnear, D. Burnand, M. J. Clift, A. F. Kilbinger, B. Rothen Rutishauser and A. Petri-Fink, *Angew. Chem. Int. Ed.,* 2014, **53**, 12613-12617.

37) B. P. Khanal and E. R. Zubarev, *Angew. Chem. Int. Ed.,* 2007, **46**, 2195-2198.

38) B. Thierry, J. Ng, T. Krieg and H. J. Griesser, *Chem.Commun.,* 2009, , 1724-1726.

39) C. Kinnear, H. Dietsch, M. J. Clift, C. Endes, B. Rothen-Rutishauser and A. Petri-Fink, *Angew. Chem. Int. Ed.,* 2013, **52**, 1934-1938.

40) V. Amendola and M. Meneghetti, *J. Phys. Chem. C,* 2009, **113**, 4277-4285.

41) J. Santillán, F. Videla, M. F. van Raap, D. Muraca, L. Scaffardi and D. Schinca, *J. Phys. D,* 2013, **46**, 435301.

42) B. T. Draine and P. J. Flatau, *JOSA A,* 1994, **11**, 1491-1499.

43) B. Draine and P. Flatau, *arxiv.org/abs/1002.1505v1 S,* .

44) V. Amendola, S. Scaramuzza, S. Agnoli, S. Polizzi and M. Meneghetti, *Nanoscale,* 2014, **6**, 1423-1433.

45) L. Cavigli, M. de Angelis, F. Ratto, P. Matteini, F. Rossi, S. Centi, F. Fusi and R. Pini, *J. Phys. Chem. C,* 2014, **118**, 16140-16146.

46) H. H. Richardson, M. T. Carlson, P. J. Tandler, P. Hernandez and A. O. Govorov, *Nano Lett.,* 2009, **9**, 1139.

47) J. Blechinger, A. T. Bauer, A. A. Torrano, C. Gorzelanny, C. Brauchle and S. W. Schneider, *Small,* 2013, **9**, 3970-3980.

48) S. George, T. Xia, R. Rallo, Y. Zhao, Z. Ji, S. Lin, X. Wang, H. Zhang, B. France and D. Schoenfeld, *ACS nano,* 2011, **5**, 1805-1817.

49) S. Gass, J. M. Cohen, G. Pyrgiotakis, G. A. Sotiriou, S. E. Pratsinis and P. Demokritou, *ACS Sust. Chem. Eng.,* 2013, **1**, 843-857.

50) S. Sharifi, S. Behzadi, S. Laurent, M. L. Forrest, P. Stroeve and M. Mahmoudi, *Chem. Soc. Rev.,* 2012, **41**, 2323-2343.

51) A. M. Dwivedi, *Drugs,* 1987, **4**, 220-229.

52) M. Longmire, P. L. Choyke and H. Kobayashi, 2008, .

53) S. Tang, M. Chen and N. Zheng, *Small,* 2014, **10**, 3139-3144.

54) S. Hashimoto, D. Werner and T. Uwada, *J. Photochem. Photobiol. C,* 2012, **13**, 28-54.

55) F. Giammanco, E. Giorgetti, P. Marsili and A. Giusti, *J. Phys. Chem. C,* 2010, **114**, 3354-3363.

56) M. Shoji, K. Miyajima and F. Mafune, *J. Phys. Chem. C,* 2008, **112**, 1929-1932.

57) D. D. Hickstein, F. Dollar, J. L. Ellis, K. J. Schnitzenbaumer, K. E. Keister, G. M. Petrov, C. Ding, B. B. Palm, J. A. Gaffney and M. E. Foord, *ACS nano,* 2014, **8**, 8810-8818.

58) V. Amendola and M. Meneghetti, *J. Mater. Chem.,* 2007, **17**, 4705-4710.

59) P. Grua, J. Morreeuw, H. Bercegol, G. Jonusauskas and F. Vallée, *Phys. Rev. B,* 2003, **68**, 035424.

60) J. Wang, P. Neogi and D. Forciniti, *J. Chem. Phys.,* 2006, **125**, 194717.

61) A. Y. Sinyagin, A. Belov, Z. Tang and N. A. Kotov, *J. Phys. Chem. B,* 2006, **110**, 7500-7507.

62) J. R. Lackowicz, *Principles of Fluorescence Spectroscopy*, Springer, 2006.

63) V. Amendola and M. Meneghetti, *Phys. Chem. Chem. Phys.,* 2013, **15**, 3027-3046.

64) A. B. Taylor, A. M. Siddiquee and J. W. Chon, *ACS nano,* 2014, **8**, 12071-12079.

65) F. Mafuné, J. Kohno, Y. Takeda and T. Kondow, *J. Phys. Chem. B,* 2003, **107**, 12589-12596.

66) F. Mafuné, J. Kohno, Y. Takeda and T. Kondow, *J. Phys. Chem. B,* 2001, **105**, 9050-9056.

67) Z. Yin, W. Zhang, Q. Fu, H. Yue, W. Wei, P. Tang, W. Li, W. Li, L. Lin and G. Ma, *Small,* 2014, **10**, 3619-3624.

68) J. M. Santillán, van Raap, Marcela B Fernández, P. M. Zélis, D. Coral, D. Muraca, D. C. Schinca and L. B. Scaffardi, *J. Nanop. Res.,* 2015, **17**, 1-13.

69) N. Matsuo, H. Muto, K. Miyajima and F. Mafuné, *Phys. Chem. Chem. Phys.,* 2007, **9**, 6027-6031.

70) J. Liao, Y. Zhang, W. Yu, L. Xu, C. Ge, J. Liu and N. Gu, *Colloids Surf. Physicochem. Eng. Aspects,* 2003, **223**, 177-183.

71) H. Zhang and D. Wang, *Angew. Chem. Int. Ed.,* 2008, **120**, 4048-4051.

72) A. N. Shipway, M. Lahav, R. Gabai and I. Willner, *Langmuir,* 2000, **16**, 8789-8795.

73) J. Widegren and L. Bergström, *J. Europ. Ceram. Soc.,* 2000, **20**, 659-665.

74) G. Wang, P. Sarkar and P. S. Nicholson, *J. Am. Ceram. Soc.,* 1997, **80**, 965-972.

75) H. Muto, K. Yamada, K. Miyajima and F. Mafuné, *J. Phys. Chem. C,* 2007, **111**, 17221-17226.

76) J. Sylvestre, S. Poulin, A. V. Kabashin, E. Sacher, M. Meunier and J. H. Luong, *J. Phys. Chem. B,* 2004, **108**, 16864-16869.

77) K. Saitow, T. Yamamura and T. Minami, *J. Phys. Chem. C,* 2008, **112**, 18340-18349.

78) E. B. Gordon, A. V. Karabulin, A. A. Morozov, V. I. Matyushenko, V. D. Sizov and I. I. Khodos, *J. Phys. Chem. Lett.,* 2014, **5**, 1072-1076.

79) V. Amendola, M. Meneghetti, S. Fiameni, S. Polizzi, G. Fracasso, A. Boscaini and M. Colombatti, *Anal. Meth.,* 2011, **3**, 849-856.

80) V. Amendola and M. Meneghetti, *Adv. Funct. Mater.,* 2012, **22**, 353-360.